Int. J. Solids Structures Vol. 24, No. 3, pp. 251–270, 1988
Printed in Great Britain.

0020–7683/88 $3.00 + .00
Pergamon Press plc

DYNAMIC RESPONSE OF A RIGID PLASTIC CLAMPED BEAM STRUCK BY A MASS AT ANY POINT ON THE SPAN

J. H. LIU† and NORMAN JONES
Department of Mechanical Engineering, University of Liverpool, P.O. Box 147, Liverpool L69 3BX, U.K.

(*Received* 1 *June* 1987)

Abstract—Theoretical analyses are presented which examine the transverse shear and bending response and the influence of finite deflections on the behaviour of rigid, perfectly plastic clamped beams struck transversely by a mass at any point on the span. It transpires that the transverse shear force may dominate the entire response when the impact point is close to the support. However, the membrane force also plays an important role when the transverse deformation is larger than the beam thickness, approximately.

NOTATION

B	width of beam
D	defined by eqn (18)
G	mass of striker
H	thickness of beam
M	bending moment
M_0	fully plastic bending moment of cross-section
N	membrane force
N_0	fully plastic membrane force of cross-section
Q	shear force
Q_0	fully plastic transverse shear force of cross-section
Q_{10}, Q_{20}	shear forces at the right- and left-hand side of section adjacent to the impact point, respectively
T	time
V_0	initial impact velocity
W	transverse displacement of beam
$\bar{W}$	W/l_1
W_0	transverse displacement at the impact point
W_{01}	displacement at the impact point when the travelling plastic hinge on the right-hand side reaches the right-hand support
W_{02}	displacement at the impact point when the travelling plastic hinge on the left-hand side reaches the left-hand support
W_1, W_2	transverse displacements at the right- and left-hand side of beam adjacent to the impact point, respectively
W_{1s}, W_{2s}	shear sliding displacements at the right- and left-hand side of the impact point, respectively
W_f	maximum permanent deformation
a_1, a_2	location of the travelling plastic hinges on the right- and left-hand sides of a beam, respectively
$f(z_2)$	defined by eqn (20b)
g	ml_1/G
m	mass per unit length of beam
q, q_{10}, q_{20}	$Q/Q_0, Q_{10}/Q_0, Q_{20}/Q_0$
r	l_1/l_2
t	M_0T/GV_0l_1
t_1, t_2	times when right- and left-hand travelling hinges reach the right- and left-hand supports, respectively
t_s	time when shear sliding ceases
t_{s1}, t_{s2}	times when shear sliding ceases at right- or left-hand side of the impact point ($t_{s1} < t_{s2}$)
t_f	time when displacement of beam ceases
u	$GV_0^2/2M_0$
x	axial coordinate
z	x/l_1
z_1, z_2	$a_1/l_1, a_2/l_1$
γ	$N_0l_1/4M_0$
σ_0	static yield stress
v_1, v_2	$Q_0l_1/2M_0, Q_0l_2/2M_0$
l	half span of beam
l_1, l_2	lengths of parts of beam defined in Fig. 2(a) ($l_1 \leqslant l_2$)
$\dot{(\,)}, (\,)'$	$\partial(\,)/\partial t$.

† On leave from Huazhong University of Science and Technology, Wuhan, China.

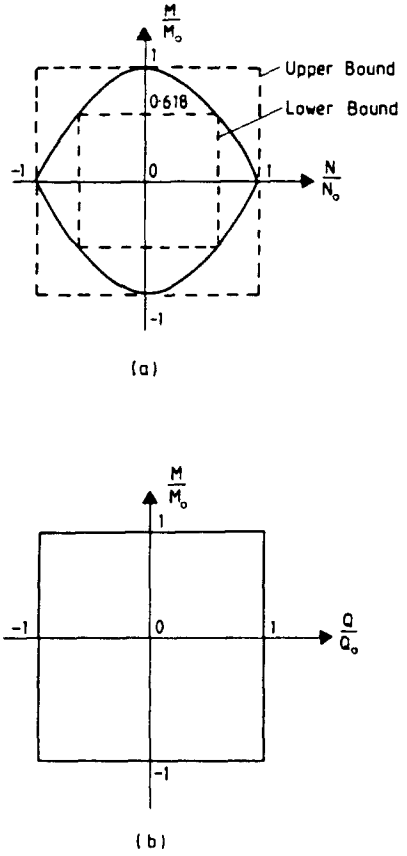

Fig. 1. Plastic yield conditions.

1. INTRODUCTION

It has been demonstrated in previous work that the transverse shear force may exercise a more important influence on the response of dynamically loaded rigid, perfectly plastic structures than in the corresponding static loading cases[1]. The initial transverse shear forces according to classical (bending only) theories are infinitely large at the boundaries of loaded zones in rigid, perfectly plastic beams, plates and shells subjected to an impulsive loading[2–5] or struck by a mass[6–8]. By way of contrast, the transverse shear forces in a statically loaded structure are finite in order to satisfy the transverse equilibrium conditions. Indeed beams, for example, may fail due to excessive transverse shear force at the supports when subjected to impulsive velocities[9] or at the impact point when struck by a mass[10]. Transverse shear effects play an important role in a structure which responds with higher modal deformation forms[11] and dominate the behaviour of ideal fibre-reinforced beams[12] and plates[13].

When a rigid, perfectly plastic beam with axial restraints at its supports is subjected to a large dynamic load, a significant discrepancy is observed between experimental results and a theoretical analysis which ignores the influence of finite deflections[7, 10, 14]. In this case, the membrane force plays an important role in the beam behaviour. A fully clamped beam may enter a string state when the maximum transverse deformation is larger than the beam thickness, approximately[7, 14, 15]. Symonds and Mentel[15] and other authors[10, 14, 16] assume that the membrane force N is constant throughout a beam which is suggested by the in-plane equilibrium equations when axial inertia is neglected. In order to simplify theoretical analyses, some authors[10, 14–16] have employed the approximate square yield curve in Fig. 1(a) instead of the more exact parabolic yield curve which is also shown in Fig. 1(a). It transpires that theoretical solutions using approximate square yield curves

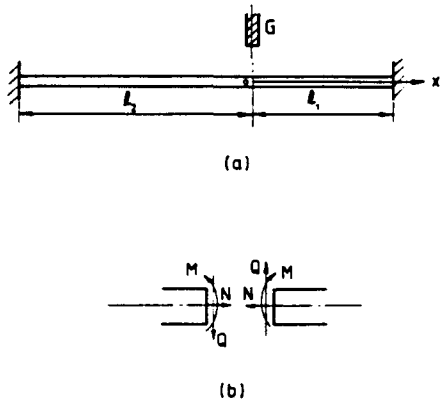

Fig. 2. Clamped beam struck transversely by a mass G.

appear to bound those relating to the parabolic yield curve and also give good agreement with the corresponding experimental results[10, 14, 16].

The dynamic response of a rigid, perfectly plastic clamped beam due to an impact loading has been examined by several authors[6, 7, 17]. The extension of this work to examine the shear and bending response and the influence of finite deflections on a clamped beam struck transversely by a mass at any point of its span, as shown in Fig. 2, is presented in Sections 2 and 3 of this paper for some particular cases which correspond to the experimental tests conducted recently in the Department of Mechanical Engineering at the University of Liverpool.†

The beam has a length $l_1 + l_2 = 2l$ and mass m per unit length and is struck at a point l_1 from the right-hand support by a mass G travelling with an initial velocity V_0 as shown in Fig. 2. After impact, the striker G is assumed to remain in contact with the beam. Therefore, the striker and the struck point of the beam have an initial velocity V_0 at the instant of contact and a common velocity throughout the entire response. Without loss of generality, the dimension l_1 can be taken smaller than l_2.

2. SHEAR AND BENDING RESPONSE OF A RIGID, PERFECTLY PLASTIC CLAMPED BEAM STRUCK TRANSVERSELY BY A MASS AT ANY POINT IN ITS SPAN

The plastic yielding of a beam is controlled by the square yield curve relating the transverse shear force and bending moment as shown in Fig. 1(b) [8, 17]. It is evident from Refs [7, 8, 17] that the transverse velocity profile of a beam may change with the magnitude $v_1 = Q_0 l_1/2M_0$ or $v_2 = Q_0 l_2/2M_0$ when the finite shear strength of a material is considered. The membrane force is neglected in this section, i.e. $N = 0$.

2.1. *Basic equations*

It is assumed that a stationary plastic bending hinge develops at the impact point $x = 0$ with two travelling bending hinges at $x = a_1$ and $-a_2$ which move towards the supports when a beam is struck by a mass G. The two parts of a beam between the stationary plastic hinge and the travelling hinges rotate as rigid bodies about the travelling hinges while the rest of a beam beyond the travelling hinges remains undeformed. This velocity profile is shown in Fig. 3(a) and may be written

$$\dot{W}(z) = \begin{cases} 0, & -1/r \leqslant z \leqslant -z_2^- \\ \dot{W}_2(1 + z/z_2), & -z_2^+ \leqslant z \leqslant 0^- \\ \dot{W}_0, & z = 0 \\ \dot{W}_1(1 - z/z_1), & 0^+ \leqslant z \leqslant z_1^- \\ 0, & z_1^+ \leqslant z \leqslant 1 \end{cases} \tag{1a–e}$$

† The experimental results will be reported in a subsequent paper.

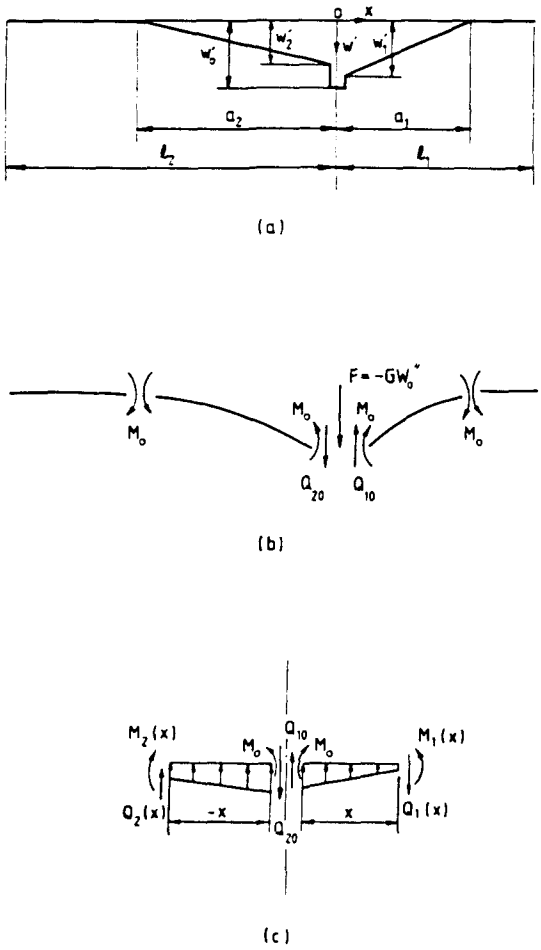

Fig. 3. Motion of a beam with two travelling plastic bending hinges, one stationary plastic bending hinge and two transverse shear slides.

where

$$z = x/l_1, \quad z_1 = a_1/l_1, \quad z_2 = a_2/l_1, \quad r = l_1/l_2 \tag{2a-d}$$

$$\bar{W} = \dot{W}/l_1, \quad (\dot{}) = \partial(\ )/\partial t, \quad t = M_0 T/GV_0 l_1 \tag{2e-g}$$

$\dot{W}_0$ is the dimensionless velocity at the impact point and $\dot{W}_1$ and $\dot{W}_2$ are the dimensionless velocities on the right- and left-hand sides adjacent to the impact point, respectively, i.e. $\dot{W} = \dot{W}_1$ at $z = 0^+$ and $\dot{W} = \dot{W}_2$ at $z = 0^-$.

The transverse and moment equilibrium equations for the regions $0^+ \leqslant z \leqslant z_1^-$ and $-z_2^+ \leqslant z \leqslant 0^-$ in Fig. 3(b) together with the transverse equilibrium equation at the impact point are

$$z_1\ddot{W}_1 + \dot{W}_1\dot{z}_1/2 = -12u(1+q_{10}v_1z_1)/gz_1 \tag{3a}$$

$$z_1\ddot{W}_1 + \dot{W}_1\dot{z}_1 = -8uv_1q_{10}/g \tag{3b}$$

$$z_2\ddot{W}_2 + \dot{W}_2\dot{z}_2/2 = -12u(1-q_{20}v_1z_2)/gz_2 \tag{3c}$$

$$z_2\ddot{W}_2 + \dot{W}_2\dot{z}_2 = 8uv_1q_{20}/g \tag{3d}$$

and

$$-q_{10}+q_{20} = -\ddot{W}_0/4uv_1 \tag{3e}$$

since the transverse shear force is zero at the plastic bending hinges and where

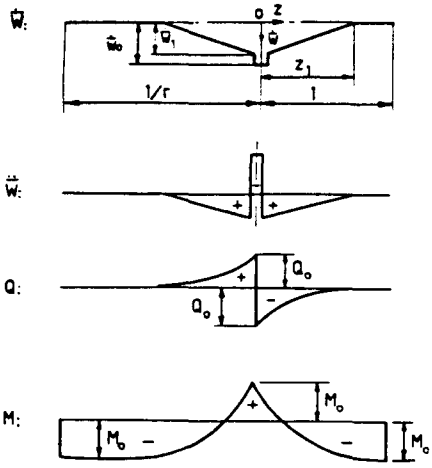

Fig. 4. First phase of motion for shear and bending response with $3 < v_1 \leqslant v_2$ (Case I).

$$v_1 = Q_0 l_1/2M_0, \quad u = GV_0^2/2M_0, \quad g = ml_1/G \quad \text{and} \quad q = Q/Q_0. \tag{4a–d}$$

2.2. *Case* I, $3 < v_1 \leqslant v_2$

2.2.1. *Phase* 1, $0 \leqslant t < t_s$. It is evident from Refs [7, 8, 17] that after impact, transverse shear sliding occurs on both sides of the impact point ($z = 0^+$ and 0^-) where the dimensionless shear forces $q_{10} = -q_{20} = -1$. A stationary plastic bending hinge is formed at $z = 0$ while two stationary plastic bending hinges develop at $z = z_1 < 1$ and $z = -z_2 > -1/r$ when $3 < v_1 \leqslant v_2$. The associated transverse velocity profile is shown in Fig. 4 and is described by eqns (1).

Equations (3) with $q_{10} = -q_{20} = -1$ and $\dot{z}_1 = \dot{z}_2 = 0$ give

$$z_1^2 \ddot{W}_1 = -12u(1 - v_1 z_1)/g \tag{5a}$$

$$z_1 \ddot{W}_1 = 8uv_1/g \tag{5b}$$

$$z_2^2 \ddot{W}_2 = -12u(1 - v_1 z_2)/g \tag{5c}$$

$$z_2 \ddot{W}_2 = 8uv_1/g \tag{5d}$$

and

$$\ddot{W}_0 = -8uv_1. \tag{5e}$$

Now, solving eqns (5), we obtain $z_2 = z_1$, $\dot{W}_2 = \dot{W}_1$, $W_2 = W_1$

$$z_1 = 3/v_1, \quad \dot{W}_1 = 8v_1^2 ut/3g, \quad \dot{W}_0 = 2u - 8uv_1 t \tag{6a–c}$$

$$W_1 = 4v_1^2 ut^2/3g, \quad W_0 = 2ut - 4uv_1 t^2 \tag{6d, e}$$

when satisfying the initial conditions $\dot{W}_1 = \dot{W}_2 = 0$, $W_1 = W_2 = 0$, $\dot{W}_0 = 2u$ and $W_0 = 0$ at $t = 0$.

Transverse shear sliding ceases when $\dot{W}_1 = \dot{W}_2 = \dot{W}_0$ which occurs at

$$t_s = 3g/\{4v_1(v_1 + 3g)\}. \tag{7}$$

It may be shown that the transverse deformations in the beam at time t_s are

$$W_0(t_s) = 3ug(v_1 + 3g/2)/\{2v_1(v_1 + 3g)^2\} \tag{8a}$$

$$W_1(t_s) = W_2(t_s) = 3ug/\{4(v_1 + 3g)^2\} \tag{8b}$$

and

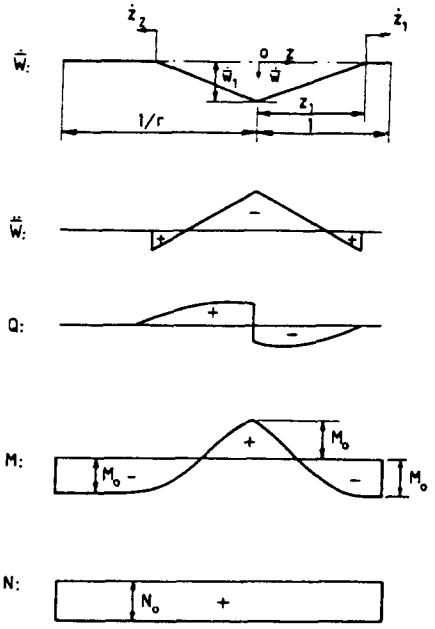

Fig. 5. Second phase of motion for shear and bending response in Case I ($N = 0$ along the beam), or first phase of motion for dynamic response with the influence of finite deflections ($N = N_0$ and $v_2 \geqslant v_1 \to \infty$).

$$\bar{W}_{1s} = \bar{W}_{2s} = \bar{W}_0(t_s) - \bar{W}_1(t_s) = 3ug/\{4v_1(v_1+3g)\} \tag{8c}$$

where $\bar{W}_{1s}$ and $\bar{W}_{2s}$ are the transverse shear sliding accumulated during this phase on the right- and left-hand side of the impact point, respectively.

2.2.2. *Phase* 2, $t_s < t \leqslant t_1$. It is observed that $\dot{W}_0 = \dot{W}_1 = \dot{W}_2$ and $z_1 = z_2$ at the end of phase 1. It is now assumed that z_1 and z_2 are a function of time t during this phase which leads to the transverse velocity profile shown in Fig. 5.

Equations (3) with $z_1 = z_2$, $q_{10} = -q_{20}$ and $\dot{W}_0 = \dot{W}_1 = \dot{W}_2$ give

$$(\dot{W}_1 z_1^2)' = 24u/g \tag{9a}$$

and

$$(1+z_1 g)\dot{W}_1 = 2u \tag{9b}$$

when using $z_1 = 3/v_1$ and $\dot{W}_1 = 2uv_1/(v_1+3g)$ at $t = t_s$.

Equations (9) can be rewritten

$$\ddot{W}_1(1-4u^2/\dot{W}_1^2) - 24ug = 0 \tag{10a}$$

and

$$gz_1^2/(1+z_1 g) = 12t. \tag{10b}$$

When $z_1 = 1$, eqns (10b) and (9b) give

$$t_1 = g/\{12(1+g)\} \tag{11a}$$

and

$$\dot{W}_1(t_1) = 2u/(1+g). \tag{11b}$$

Integrating eqn (10a) after multiplying by $\dot{W}_1$, we obtain

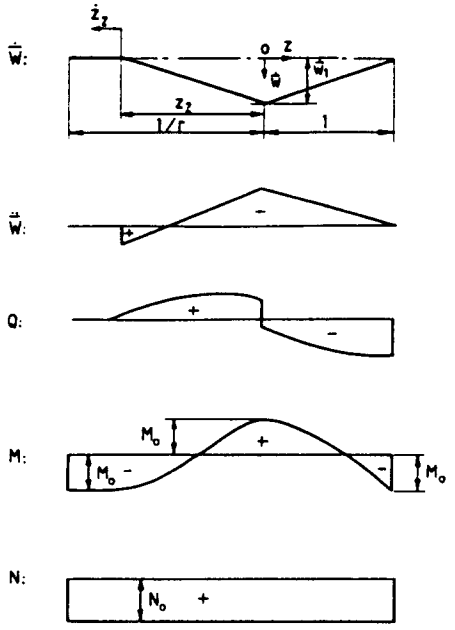

Fig. 6. Third phase of motion for shear and bending response in Case I, or second phase of motion with the influence of finite deflections.

$$\dot{W}_1^2/2 - 4u^2 \ln(\dot{W}_1) - 24ug\dot{W}_1 = A \tag{12a}$$

where

$$A = \dot{W}_1^2(t_s)/2 - 4u^2 \ln[\dot{W}_1(t_s)] - 24ug\dot{W}_1(t_s)$$

or

$$A = 2u^2(v_1 - 3g)/(v_1 + 3g) - 4u^2 \ln[2uv_1/(v_1 + 3g)]. \tag{12b}$$

Substituting eqn (11b) into eqns (12) gives

$$\dot{W}_1(t_1) = \dot{W}_2(t_1) = u\{1/(1+g)^2 - (v_1 - 3g)/(v_1 + 3g) - 2 \ln[(v_1 + 3g)/(v_1 + v_1 g)]\}/12g. \tag{13}$$

2.2.3. *Phase* 3, $t_1 < t \leqslant t_2$. The right-hand travelling plastic hinge reaches the right-hand support at $t = t_1$ where it remains throughout this phase of motion. Thus, $z_1 = 1$, $\dot{z}_1 = 0$ and $\dot{W}_0 = \dot{W}_1 = \dot{W}_2$ and the associated transverse velocity profile is shown in Fig. 6.

Equations (3a) and (3c)–(3e) with $z_1 = 1$, $\dot{z}_1 = 0$ and $\dot{W}_0 = \dot{W}_1 = \dot{W}_2$ predict

$$g(\dot{W}_1 z_2^2)'/12u = 2 \tag{14a}$$

and

$$g(z_2\dot{W}_1)'/4u = -(3+g)\ddot{W}_1/6u - 2 \tag{14b}$$

which, when integrated become

$$g\dot{W}_1 z_2^2/12u = 2(t - t_1) + B \tag{15a}$$

and

$$(3gz_2 + 6 + 2g)\dot{W}_1/12u = -2(t - t_1) + C \tag{15b}$$

respectively, where

$$B = g\dot{W}_1(t_1)z_2^2(t_1)/12u \quad \text{and} \quad C = [gz_2(t_1)/4u + 1/2u + g/6u]\dot{W}_1(t_1). \tag{15c, d}$$

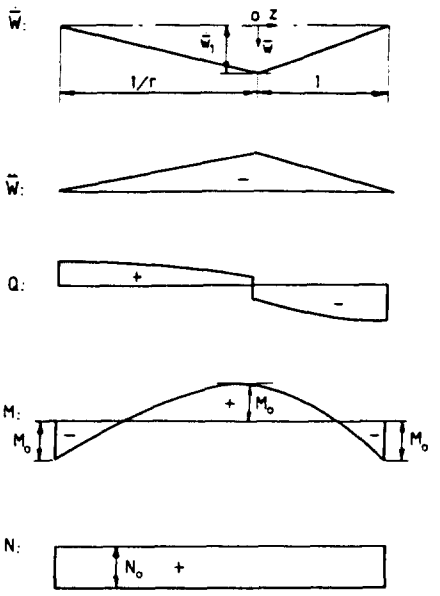

Fig. 7. Final phase of motion for shear and bending response in Case I, or final phase of motion with the influence of finite deflections.

Equations (15) predict that

$$\dot{\bar{W}}_1 = 12u(B+C)/D \tag{16}$$

while eqns (14a) and (16) give

$$\dot{z}_2 = 2D^2/[gz_2(3gz_2+12+4g)(B+C)] \tag{17}$$

where

$$D = gz_2^2+3gz_2+6+2g. \tag{18}$$

Now, $\dot{\bar{W}}_1 = \dot{z}_2 \partial \bar{W}_1/\partial z_2$, which using eqns (16) and (17), becomes

$$\partial \bar{W}_1/\partial z_2 = 6ugz_2(3gz_2+12+4g)(B+C)^2/D^3. \tag{19}$$

It may be shown when integrating eqn (19) that

$$\bar{W}_1 = 0.5ug(B+C)^2\{(36z_2+54)/[D(g-24)] - (18z_2+12+36/g)/D^2 + 3f(z_2)/(g-24)\}\Big|_{z_2(t_1)}^{z_2} + \bar{W}_1(t_1) \tag{20a}$$

where

$$f(z_2) = \begin{cases} \dfrac{24}{\sqrt{(g(24-g))}} \arctan\left[\dfrac{2gz_2+3g}{\sqrt{(g(24-g))}}\right] & \text{for } g < 24 \\ \dfrac{12}{\sqrt{(g(g-24))}} \ln\left[\dfrac{2gz_2+3g-\sqrt{(g(g-24))}}{2gz_2+3g+\sqrt{(g(g-24))}}\right] & \text{for } g > 24 \end{cases} \tag{20b}$$

and B, C and D are defined by eqns (15c), (15d) and (18), respectively.

2.2.4. *Phase* 4, $t_2 < t \leqslant t_f$. The left-hand side travelling plastic hinge at $z = -z_2$ reaches the left-hand support at $t = t_2$ after which the two parts of the beam rotate as rigid bodies until all the initial kinetic energy has been dissipated as plastic work. The transverse velocity profile during this final phase of motion is shown in Fig. 7.

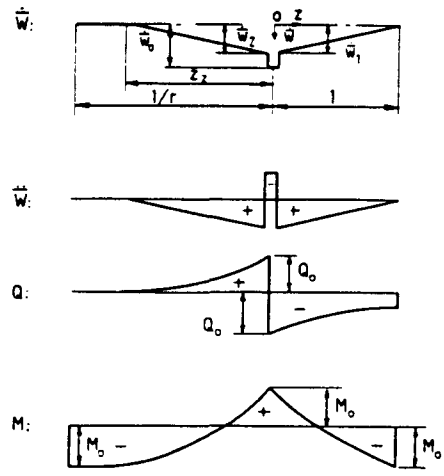

Fig. 8. First phase of motion for shear and bending response with $1 < v_1 \leqslant 3$ and $v_2 > 3$ (Case II).

Equations (3a), (3c), and (3e) with $z_1 = 1, \dot{z}_1 = 0, z_2 = 1/r, \dot{z}_2 = 0$ and $\dot{W}_0 = \dot{W}_1 = \dot{W}_2$ give

$$[(1+r)g/3+r]\ddot{W}_1 = -4ur(1+r) \tag{21}$$

which may be integrated to predict

$$\dot{W}_1 = -4ur(1+r)(t-t_2)/[r+(1+r)g/3] + \dot{W}_1(t_2) \tag{22a}$$

and

$$W_1 = -2ur(1+r)(t-t_2)^2/[r+(1+r)g/3] + \dot{W}_1(t_2)(t-t_2) + W_1(t_2). \tag{22b}$$

Motion ceases at $t = t_f$ when $\dot{W} = 0$ and, therefore

$$t_f = \dot{W}_1(t_2)[r+(1+r)g/3]/[4ur(1+r)] + t_2 \tag{23a}$$

with an associated permanent transverse deformation of the beam

$$W_{1f} = [r+(1+r)g/3]\dot{W}_1^2(t_2)/[8ur(1+r)] + W_1(t_2) \tag{23b}$$

where $\dot{W}_1(t_2)$ and $W_1(t_2)$ are the respective velocity and deformation at the right-hand side of the impact point when $t = t_2$.

The maximum permanent transverse deformation at the impact point is

$$W_f = W_{1f} + W_{1s} \tag{23c}$$

where W_{1s} is given by eqn (8c) and is the shear sliding deformation at the right-hand side of the impact point.

2.3. *Case* II, $1 < v_1 \leqslant 3$ *and* $3 < v_2$

Equation (6a) shows that if $v_1 < 3$ then $z_1 \geqslant 1$ and the velocity profile in Fig. 4 is no longer valid. Therefore, it is assumed that a stationary plastic hinge occurs at the right-hand support for beams having $v_1 \leqslant 3$ as shown in Fig. 8.

2.3.1. *Phase* 1, $0 \leqslant t \leqslant t_{s1}$. After impact, the mechanics of motion are the same as those in Section 2.2.1 except the right-hand plastic bending hinge now remains at the right-hand support where $z = 1$ as shown in Fig. 8.

Equations (3a) and (3c)–(3e) with $z_1 = 1, \dot{z}_1 = 0, q_{10} = -1, q_{20} = 1$ and $\dot{z}_2 = 0$ give

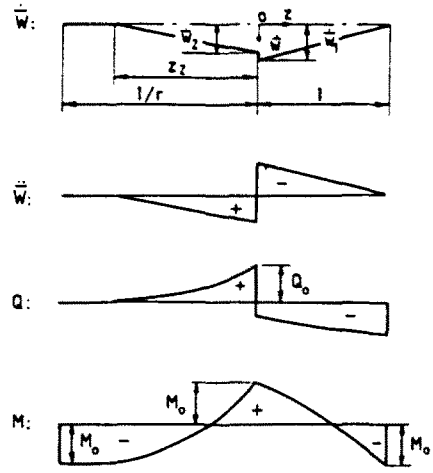

Fig. 9. Case II with $1.5 \leqslant v_1 < 3$ for $t_{s1} < t \leqslant t_{s2}$.

$$z_2 = 3/v_1, \quad \dot{W}_0 = 2u - 8v_1 ut, \quad \dot{W}_1 = 12u(v_1 - 1)t/g \tag{24a–c}$$

$$\dot{W}_2 = 8uv_1^2 t/3g, \quad W_0 = 2ut - 4uv_1 t^2, \quad W_1 = -6u(1 - v_1)t^2/g \tag{24d–f}$$

and

$$W_2 = 4uv_1^2 t^2/3g \tag{24g}$$

since $\dot{W}_0 = 2u$, $\dot{W}_1 = \dot{W}_2 = 0$ and $W_0 = W_1 = W_2 = 0$ at $t = 0$. It is evident from eqns (24c) and (24d) that $\dot{W}_1 \geqslant \dot{W}_2$ when $3/2 \leqslant v_1 \leqslant 3$. Therefore, the shear sliding on the right-hand side of the impact point first stops if $3/2 \leqslant v_1 \leqslant 3$, while the left-hand side ceases at an earlier time when $1 < v_1 < 3/2$. Equations (24) for $3/2 \leqslant v_1 \leqslant 3$, give $\dot{W}_0 = \dot{W}_1$ at

$$t_{s1} = g/\{4v_1 g - 6(1 - v_1)\} \quad \text{and} \quad W_{1s} = ug/\{4v_1 g - 6(1 - v_1)\} \tag{25a, b}$$

while for $1 < v_1 < 3/2$, $\dot{W}_0 = \dot{W}_2$ at

$$t_{s1} = 3g/\{4v_1(v_1 + 3g)\} \quad \text{and} \quad W_{2s} = 3ug/\{4v_1(v_1 + 3g)\}. \tag{26a, b}$$

2.3.2. *Phase* 2, $t_{s1} < t \leqslant t_{s2}$. It was found in the previous section for $3/2 \leqslant v_1 \leqslant 3$ that shear sliding stops at $z = 0^+$ when $t = t_{s1}$, while the other transverse shear slide at $z = 0^-$ continues and gives the velocity profile shown in Fig. 9. Equations (3a) and (3c)–(3e) with $\dot{W}_0 = \dot{W}_1$, $q_{20} = 1$, $z_1 = 1$, $\dot{z}_1 = 0$ and $\dot{z}_2 = 0$ give

$$\dot{W}_1 = -12u(1 + v_1)t/(3 + g) + 6u/(3 + g), \quad \dot{W}_2 = 8uv_1^2 t/3g, \quad z_2 = 3/v_1 \tag{27a–c}$$

$$W_1 = -6u(1 + v_1)t^2/(3 + g) + 6ut/(3 + g) - 3ug/\{2(3 + g)(2v_1 g - 3 + 3v_1)\} \tag{27d}$$

$$W_2 = 4uv_1^2 t^2/3g \tag{27e}$$

and

$$\dot{W}_2 = \dot{W}_1 \quad \text{at} \quad t_{s2} = 9g/(12v_1^2 + 4v_1^2 g + 18g + 18v_1 g). \tag{27f}$$

The subsequent motion is the same as phases 3 and 4 in Case I with t_1, $z_2(t_1)$ and $\dot{W}_1(t_1)$ replaced by t_{s2}, $3/v_1$ and $\dot{W}_1(t_{s2})$, respectively.

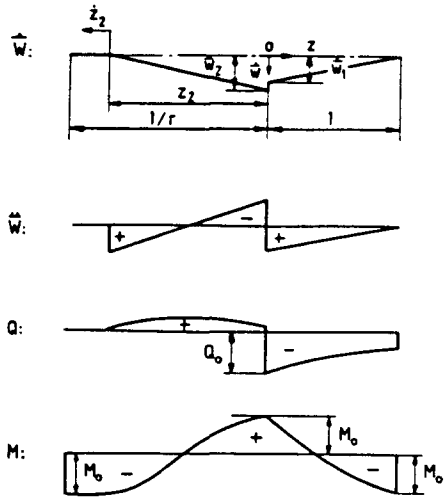

Fig. 10. Case II with $1 < v_1 < 1.5$ for $t_{s1} < t \leqslant t_{s2}$.

For $1 < v_1 < 3/2$, shear sliding ceases at $z = 0^-$ when $t = t_{s1}$, while shearing continues at $z = 0^+$ as shown in Fig. 10. Equations (3a) and (3c)–(3e) with $\dot{W}_0 = \dot{W}_2$, $q_{10} = -1$, $z_1 = 1$ and $\dot{z}_1 = 0$ give

$$\dot{W}_1 = 12u(v_1 - 1)t/g, \quad \bar{W}_1 = 6u(v_1 - 1)t^2/g \tag{28a, b}$$

$$g\dot{W}_2 z_2^2/12u = 2t \quad \text{and} \quad (2+gz_2)\dot{W}_2/8uv_1 = 1/2v_1 - t \tag{28c, d}$$

which may be rearranged in the form

$$\dot{W}_2 = 12u/(v_1 g z_2^2 + 6 + 3gz_2) \tag{29a}$$

or

$$\dot{W}_2 = 2u + 3ugt - 4uv_1 t - u\sqrt{(3gt(3gt - 8v_1 t + 4))} \tag{29b}$$

and

$$t = gz_2^2/(2v_1 gz_2^2 + 12 + 6gz_2). \tag{29c}$$

Now, integrating eqn (29b) with respect to time t, we obtain

$$\bar{W}_2 = [2ut + 3ugt^2/2 - 2v_1 ut^2 - (2at+b)\sqrt{(t(at+b))}/4a + f(t)]|_{t_{s1}}^{t} + \bar{W}_2(t_{s1}) \tag{30a}$$

where

$$a = gu^2(9g - 24v_1), \quad b = 12gu^2 \tag{30b, c}$$

and

$$f(t) = \begin{cases} b^2(8a\sqrt{a})^{-1} \ln [2at + b + 2\sqrt{(at(at+b))}] & \text{for } a > 0 \\ b^2(8a\sqrt{-a})^{-1} \arcsin [-(2at+b)/b] & \text{for } a < 0. \end{cases} \tag{30d}$$

Equations (28a) and (28c) predict that

$$\bar{z}_2 = \sqrt{(2/(v_1 - 1))} \tag{31}$$

when $\dot{W}_1 = \dot{W}_2$. Therefore, two types of motion are possible depending on the magnitude of $\bar{z}_2$.

If $\bar{z}_2 < 1/r$, or $r^2 < (v_1-1)/2$, then $z_2(t_{s2}) = \bar{z}_2 = \sqrt{(2/(v_1-1))}$ and $\dot{W}_1 = \dot{W}_2$ at

$$t_{s2} = [3\sqrt{(2(v_1-1))} + 6(v_1-1)/g + 2v_1]^{-1}. \tag{32}$$

The subsequent motion is the same as phases 3 and 4 in Case I but with t_1, $z_2(t_1)$ and $\dot{W}_1(t_1)$ replaced by t_{s2}, $z_2(t_{s2})$ and $\dot{W}_1(t_{s2})$, respectively.

If $\bar{z}_2 \geqslant 1/r$, or $r^2 \geqslant (v_1-1)/2$, then the left-hand travelling plastic hinge reaches the left-hand support before shear sliding ceases at $z = 0^+$. Therefore, eqns (28)–(30) are valid until $z_2 = 1/r$ at

$$\bar{t}_2 = g/(6gr + 12r^2 + 2v_1 g). \tag{33}$$

The motion of a beam is now governed by eqns (3a), (3c) and (3e) with $q_{10} = -1$, $z_1 = 1$, $\dot{z}_1 = 0$, $z_2 = 1/r$, $\dot{z}_2 = 0$ and $\dot{\bar{W}}_0 = \dot{\bar{W}}_2$ which give

$$\dot{\bar{W}}_1 = 12u(v_1-1)t/g, \quad \dot{\bar{W}}_2 = 6u[1/r - 2(1+v_2)t]r^2/(g+3r) \tag{34a, b}$$

$$\bar{W}_1 = 6u(v_1-1)t^2/g \tag{34c}$$

and

$$\bar{W}_2 = 6ur(t-\bar{t}_2)\,[1-(r+v_1)\,(t+\bar{t}_2)]/(g+3r) + \bar{W}_2(\bar{t}_2) \tag{34d}$$

where $\bar{W}_2(\bar{t}_2)$ is obtained by substituting eqn (33) into eqn (30a).

Now, $\dot{\bar{W}}_1 = \dot{\bar{W}}_2$ and shear sliding ceases at $z = 0^+$ when

$$t_{s2} = 0.5rg/[(v_1-1)\,(g+3r) + gr^2(1+v_2)]. \tag{35}$$

The subsequent motion is the same as phase 4 of Case I but with $\dot{\bar{W}}_1(t_2)$ and $\bar{W}_1(t_2)$ replaced by $\dot{\bar{W}}_1(t_{s2})$ and $\bar{W}_1(t_{s2})$, respectively.

The final shear deformations for this case are

$$\bar{W}_{2s} = \bar{W}_1(t_{s2}) + \bar{W}_{1s} - \bar{W}_2(t_{s2}) \quad \text{if } 3/2 \leqslant v_1 \leqslant 3 \tag{36a}$$

where $\bar{W}_{1s}$ and t_{s2} are defined by eqns (25b) and (27f), respectively, and

$$\bar{W}_{1s} = \bar{W}_2(t_{s2}) + \bar{W}_{2s} - \bar{W}_1(t_{s2}) \quad \text{if } 1 < v_1 < 3/2 \tag{36b}$$

where $\bar{W}_{2s}$ and t_{s2} are defined by eqns (26b) and (32) or (35), respectively.

2.4. *Case* III, $0 < v_1 \leqslant 1$ *and* $3 < v_2$.

Equation (24c) indicates that $\dot{\bar{W}}_1 < 0$ and $\ddot{\bar{W}}_1 < 0$ when $v_1 < 1$. This is not permissible because $q_1 < q_{10} = -1$ and yield violations of the shear force would occur in $0^+ \leqslant z \leqslant 1$, if $\ddot{\bar{W}}_1 < 0$. The theoretical analysis in this section uses the velocity profile shown in Fig. 11 with the entire beam on the right-hand side of the impact point remaining stationary throughout the response.

2.4.1. *Phase* 1, $0 \leqslant t \leqslant t_{s1}$. Equations (3) with $\dot{\bar{W}}_1 = 0$ and $q_{10} = -1$ reduce to

$$(\dot{\bar{W}}_2 z_2^2)' = 24u/g \tag{37a}$$

$$q_{20} = g(\dot{\bar{W}}_2 z_2)'/8uv_1 \tag{37b}$$

and

$$q_{20} + 1 = -\ddot{\bar{W}}_0/4uv_1. \tag{37c}$$

Transverse shear slides develop at $z = 0^-$ and 0^+ after impact as shown in Fig. 11 and, therefore, eqns (37) with $q_{20} = 1$ become

$$\dot{\bar{W}}_0 = 2u - 8uv_1 t, \quad \dot{\bar{W}}_2 = 8uv_1^2 t/3g, \quad z_2 = 3/v_1 \tag{38a–c}$$

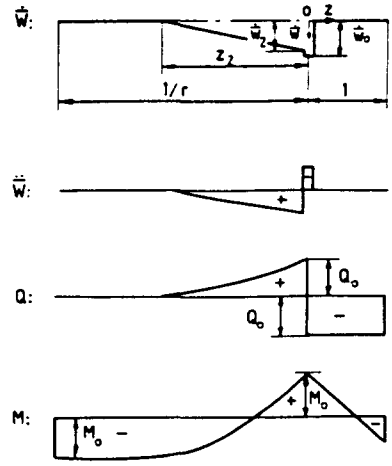

Fig. 11. First phase of motion for shear and bending response with $0 < v_1 \leqslant 1$ and $v_2 > 3$ (Case III).

$$\dot{W}_0 = 2ut - 4uv_1 t^2 \quad \text{and} \quad \dot{W}_2 = 4uv_1^2 t^2/3g \tag{38d,e}$$

since $\dot{W}_0 = 2u$, $\dot{W}_2 = 0$, $W_0 = 0$ and $W_2 = 0$ when $t = 0$. Equations (38a) and (38b) give $\dot{W}_0 = \dot{W}_2$ at

$$t_{s1} = 3g/\{4v_1(v_1 + 3g)\} \quad \text{and} \quad \dot{W}_{2s} = 3ug/\{4v_1(v_1 + 3g)\}. \tag{39a,b}$$

2.4.2. *Phase* 2, $t_{s1} < t \leqslant t_2$. The shear sliding ceases at $z = 0^-$ when $t = t_{s1}$ and the subsequent motion in Fig. 12 is still governed by eqns (37) with $\dot{W}_0 = \dot{W}_2$. Thus, eqns (28c)-(30) with t_{s1} given by eqn (39a) are valid for this case until

$$t_2 = g/(6gr + 12r^2 + 2v_1 g) \tag{40}$$

which is obtained from eqn (29c) with $z_2 = 1/r$ when the travelling plastic hinge reaches the left-hand support.

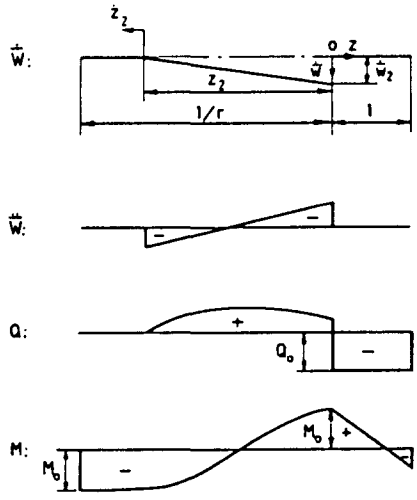

Fig. 12. Case III when $t_{s1} < t \leqslant t_2$.

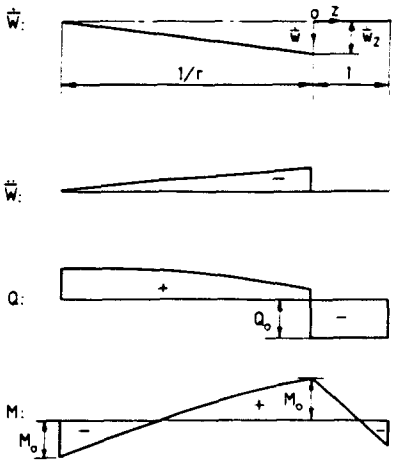

Fig. 13. Case III when $t_2 < t \leqslant t_f$.

2.4.3. *Phase* 3, $t_2 < t \leqslant t_f$. The travelling plastic hinge at $z = -z_2$ reaches the left-hand support at $t = t_2$ which is defined by eqn (40). The shear sliding at $z = 0^+$ remains active during subsequent motion as shown in Fig. 13.

Equations (3c) and (3e) with $\dot{\bar{W}}_1 = 0$, $\dot{\bar{W}}_0 = \dot{\bar{W}}_2$, $q_{10} = -1$, $z_2 = 1/r$ and $\dot{z}_2 = 0$ give

$$\dot{\bar{W}}_2 = -12u(r+v_1)r(t-t_2)/(g+3r) + \dot{\bar{W}}_2(t_2) \tag{41a}$$

and

$$\bar{W}_2 = -6u(r+v_1)r(t-t_2)^2/(g+3r) + \dot{\bar{W}}_2(t_2)(t-t_2) + \bar{W}_2(t_2) \tag{41b}$$

where

$$\dot{\bar{W}}_2(t_2) = 12ur^2/(v_1 g + 6r^2 + 3gr) \tag{41c}$$

is obtained from eqn (29a) with $z_2 = 1/r$ and $\bar{W}_2(t_2)$ is found from eqns (30) with t_{s1} and t_2 given by eqns (39a) and (40), respectively.

The response duration is calculated from eqn (41a) with $\dot{\bar{W}}_2 = 0$, or

$$t_f = 0.5/(r+v_1). \tag{42a}$$

The associated maximum permanent transverse deformation is

$$\bar{W}_{2f} = (g+3r)\dot{\bar{W}}_2^2(t_2)/\{24u(r+v_1)r\} + \bar{W}_2(t_2) \tag{42b}$$

while the shear sliding at $z = 0^+$ when motion ceases is

$$\bar{W}_{1s} = \bar{W}_{2f} + \bar{W}_{2s} \tag{43}$$

where $\bar{W}_{2s}$ is defined by eqn (39b).

3. FINITE DEFLECTION BEHAVIOUR OF A RIGID PLASTIC CLAMPED BEAM STRUCK TRANSVERSELY BY A MASS AT ANY POINT ON THE SPAN

It is suggested by previous theoretical analyses and experimental evidence[6, 18] that three phases of motion are necessary to describe the behaviour of a clamped beam struck by a mass as shown in Fig. 2(a). A stationary plastic hinge develops at the impact point $z = 0$ during the first phase, while two travelling plastic hinges originate from the impact point and travel towards the supports. The two parts of the beam between the stationary and travelling plastic hinges rotate as rigid bodies about the travelling hinges, while the

remainder of the beam remains undeformed. The second phase of motion commences at $t = t_1$ when the right-hand travelling hinge reaches the right-hand support and finishes at $t = t_2$ when the left-hand travelling hinge reaches the left-hand support. The plastic bending hinges remain stationary at the impact point and both supports during the final phase of motion.

In order to simplify theoretical analyses, which retain finite deflection effects, it is usually assumed that the membrane force N is constant throughout the span of a beam. It is well known, e.g. Refs [14–16], that the fully plastic membrane (string) state is reached when the maximum transverse displacement equals the thickness of a perfectly plastic fully clamped beam. Thus, if interest is confined to large plastic deformations, then it is reasonable to let $N = N_0$ throughout the response and use the square yield condition in Fig. 1(a). It was shown in Refs [9, 19] that transverse shear forces may exercise an important influence during the early phase of motion when the displacements are small but are less important for large displacements and are, therefore, not retained in the yield condition in this section.

3.1. *First phase*, $0 \leqslant t \leqslant t_1$

The transverse velocity profile shown in Fig. 5 may be expressed in the form

$$\dot{W} = \begin{cases} 0, & -1/r \leqslant z \leqslant -z_2^- \\ \dot{W}_0(1+z/z_2), & -z_2^+ \leqslant z \leqslant 0^- \\ \dot{W}_0, & z = 0 \\ \dot{W}_0(1-z/z_1), & 0^+ \leqslant z \leqslant z_1^- \\ 0, & z_1^+ \leqslant z \leqslant 1 \end{cases} \tag{44}$$

where $z_1 = z_2$ during this phase of motion.

The transverse and moment equilibrium equations for the beam are

$$z_1\ddot{W}_0 + \dot{W}_0\dot{z}_1 = -\ddot{W}_0/g \tag{45a}$$

and

$$gz_1^2\ddot{W}_0 + gz_1\dot{z}_1\dot{W}_0/2 + 3z_1\ddot{W}_0/2 = -12u(1+2\gamma\bar{W}_0) \tag{45b}$$

since

$$q_{10} = -q_{20} = \ddot{W}_0/8uv_1 \tag{45c}$$

where

$$\gamma = N_0l_1/4M_0.$$

Equations (45a) and (45b) can be rewritten in the form

$$(\dot{W}_0z_1^2)' = 24u(1+2\gamma\bar{W}_0)/g \tag{46a}$$

and

$$(1+gz_1)\dot{W}_0 = 2u \tag{46b}$$

because $z_1 = 0$ and $\dot{W}_0 = 2u$ when $t = 0$. Equations (46) give

$$\ddot{W}_0 - 4u^2\ddot{W}_0/\dot{W}_0^2 - 24ug - 48ug\gamma\bar{W}_0 = 0 \tag{47}$$

which integrating, after multiplying by $\dot{W}_0$, predicts

$$\dot{W}_0^2/2 - 4u^2\ln\dot{W}_0 - 24ug\bar{W}_0 - 24ug\gamma\bar{W}_0^2 = 2u^2 - 4u^2\ln(2u) \tag{48}$$

since $\bar{W}_0 = 0$ at $t = 0$.

The right-hand travelling plastic hinge reaches the right-hand support when $t = t_1$ and the associated dimensionless transverse velocity is

$$\dot{\bar{W}}_{01} = 2u/(1+g) \tag{49a}$$

according to eqn (46b), which substituting into eqn (48) gives the corresponding dimensionless transverse displacement

$$\bar{W}_{01} = \{-1+\sqrt{[1-u\gamma[g(2+g)/(1+g)^2-2\ln(1+g)]/3g]}\}/2\gamma. \tag{49b}$$

3.2. *Second phase*, $t_1 < t \leqslant t_2$

The right-hand plastic hinge remains at the right-hand support during this phase of motion, while the left-hand plastic hinge continues to travel towards the left-hand support as shown in Fig. 6, or

$$\dot{\bar{W}} = \begin{cases} 0, & -1/r \leqslant z \leqslant -z_2^- \\ \dot{\bar{W}}_0(1+z/z_2), & -z_2^+ \leqslant z \leqslant 0^- \\ \dot{\bar{W}}_0, & z = 0 \\ \dot{\bar{W}}_0(1-z), & 0^+ \leqslant z \leqslant 1. \end{cases} \tag{50}$$

The transverse and moment equilibrium equations together with the transverse equilibrium equation at the impact point $z = 0$ give

$$(\dot{\bar{W}}_0 z_2^2)' = 24u(1+2\gamma\bar{W}_0)/g \tag{51a}$$

and

$$(z_2\dot{\bar{W}}_0)' = -2\ddot{\bar{W}}_0(3+g)/3g - 8u(1+2\gamma\bar{W}_0)/g \tag{51b}$$

which may be arranged in the form

$$3(z_2\dot{\bar{W}}_0)' + (\dot{\bar{W}}_0 z_2^2)' + 2\ddot{\bar{W}}_0(3+g)/g = 0. \tag{52}$$

Integrating eqn (52) with respect to time t, we obtain

$$\dot{\bar{W}}_0 = 12u/D \tag{53a}$$

since $z_1 = z_2 = 1$ at $t = t_1$, $\dot{\bar{W}}_{01}$ is given by eqn (49a) at $t = t_1$ and where D is defined by eqn (18). Equation (52) may also be written as

$$\ddot{\bar{W}}_0 = -(3+2z_2)g\dot{\bar{W}}_0\dot{z}_2/D. \tag{53b}$$

Now, substituting eqn (53b) into eqn (51a) predicts the velocity of the travelling plastic hinge

$$\dot{z}_2 = 24u(1+2\gamma\bar{W}_0)D/\{gz_2\dot{\bar{W}}_0(3gz_2+12+4g)\} \tag{53c}$$

which with eqn (53a) gives

$$\partial\bar{W}_0/\partial z_2 = 6ugz_2(3gz_2+12+4g)/\{(1+2\gamma\bar{W}_0)D^3\} \tag{54}$$

since $\dot{\bar{W}}_0 = \dot{z}_2\partial\bar{W}_0/\partial z_2$. Finally, the dimensionless transverse displacement during this phase of motion is obtained by integrating eqn (54), or

$$\bar{W}_0+\gamma\bar{W}_0^2 = 0.5ug\{(36z_2+54)/[(g-24)D]-(18z_2+12+36/g)/D^2 + 3f(z_2)/(g-24)\}|_{z_2(t_1)}^{z_2} + \bar{W}_{01}+\gamma\bar{W}_{01}^2 \quad (55)$$

where $z_2(t_1) = 1$, $f(z_2)$ is defined by eqn (20b) and $\bar{W}_{01}$ is the displacement at the impact point when $t = t_1$ according to eqn (49b).

3.3. *Final phase*, $t_2 < t \leqslant t_f$

The left-hand travelling plastic hinge (at $z = -z_2$) reaches the left-hand support at $t = t_2$. The two parts of the beam then rotate as rigid bodies during this phase of motion until all of the initial kinetic energy is dissipated as plastic work. The associated transverse velocity profile is shown in Fig. 7, or

$$\dot{\bar{W}} = \begin{cases} \dot{\bar{W}}_0(1+zr), & -1/r \leqslant z \leqslant 0 \\ \dot{\bar{W}}_0(1-z), & 0 \leqslant z \leqslant 1. \end{cases} \quad (56)$$

It may be shown that the transverse and moment equilibrium equations of a beam reduce to the expression

$$[g(1+r)/3+r]\ddot{\bar{W}}_0+4u(1+r)r(1+2\gamma\bar{W}_0) = 0 \quad (57)$$

which, integrating after multiplying by $\dot{\bar{W}}_0$, we obtain

$$0.5[g(1+r)/3+r]\dot{\bar{W}}_0^2+4u(1+r)r(\bar{W}_0+\gamma\bar{W}_0^2) = E \quad (58a)$$

where

$$E = 0.5[g(1+r)/3+r]\dot{\bar{W}}_{02}^2+4u(1+r)r(\bar{W}_{02}+\gamma\bar{W}_{02}^2) \quad (58b)$$

and $\dot{\bar{W}}_{02}$ and $\bar{W}_{02}$ are the respective transverse velocity and displacement at the impact point when $z_2 = 1/r$ at the end of the second phase of motion ($t = t_2$).

The motion of the beam ceases when $\dot{\bar{W}}_0 = 0$ and, therefore, the maximum permanent transverse deformation at the impact point is

$$\bar{W}_f+\gamma\bar{W}_f^2 = E/[4u(1+r)r]$$

or

$$\bar{W}_f = \{-1+\sqrt{[1+E\gamma/[u(1+r)r]]}\}/2\gamma. \quad (59)$$

4. DISCUSSION

The theoretical analyses presented herein on the behaviour of clamped beams struck transversely by a mass G at any point of the span is part of a larger study. Some particular cases which correspond to the parameters which describe the experimental tests conducted in the Department of Mechanical Engineering at the University of Liverpool are presented in this paper. The experimental test results and comparisons with theoretical predictions are presented in Ref. [20].

It can be shown that the theoretical analyses in Sections 2 and 3 satisfy both the kinematic and static admissibility conditions, provided $g < 3r^2/v_1$, approximately, which embraces all the experimental test results. Otherwise, it is necessary to develop theoretical solutions with alternative transverse velocity profiles. The maximum dimensionless permanent transverse deformation and transverse shear sliding deformation for some clamped beams with rectangular cross-sections are plotted in Figs 14 and 15, where $Q_0 = BH\sigma_0/2$, $M_0 = BH^2\sigma_0/4$, $N_0 = BH\sigma_0$ and $v_1 = \gamma = l_1/H$. It is evident that the dimensionless

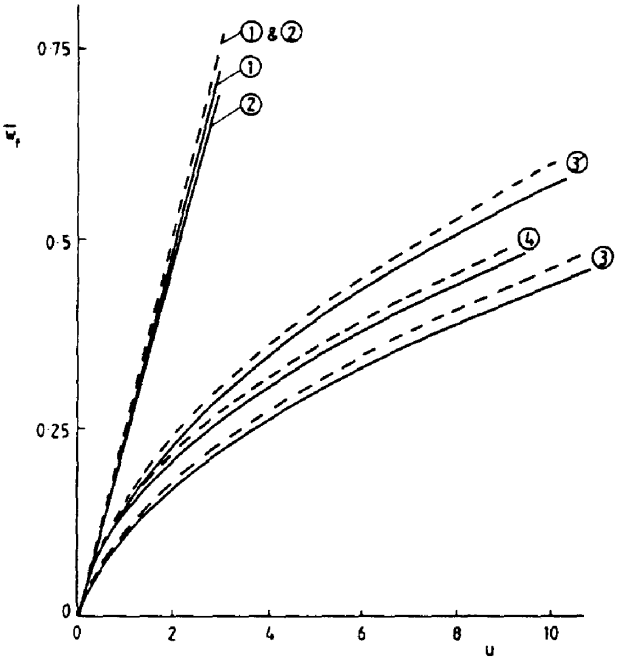

Fig. 14. Variation of $\bar{W}_f$ with u when $r = 1$ (mass strikes at the midspan) and $l_1/H = 10$ for beams with rectangular cross-sections: ——, $g = 10^{-1}$; – – –, $g = 10^{-5}$. ①, Bending only theoretical solution; ②, shear and bending theoretical solution; ③, theoretical solution with influence of finite deflections for the square yield condition in Fig. 1(a) which circumscribes the exact yield condition; ③, same as ③ except for an inscribing square yield condition which is 0.618 times as large; ④, theoretical solution of Nonaka[7] which uses the exact yield curve in Fig. 1(a).

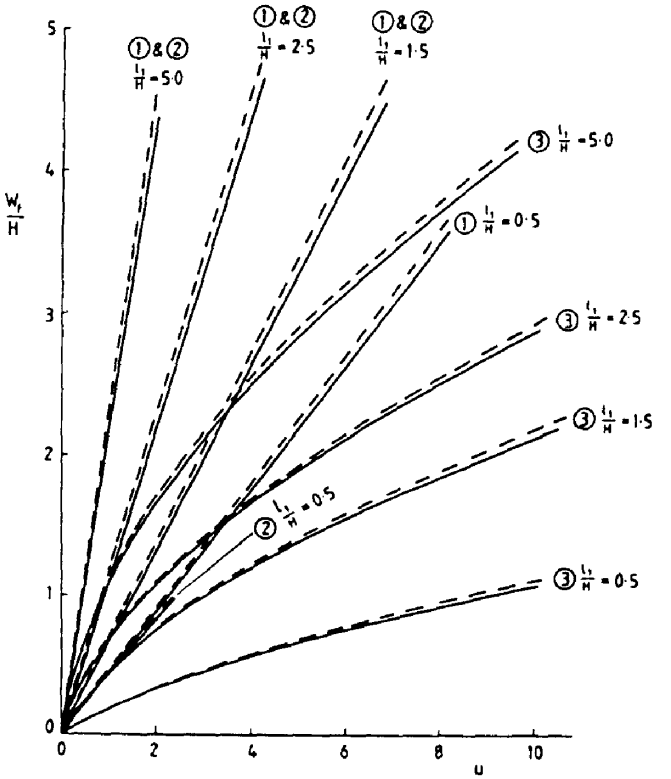

Fig. 15. Variation of W_f/H with u when $r = 0.1$. Notation is defined in the caption to Fig. 14.

maximum permanent deformation increases with the decrease of the mass ratio g, but the difference is small when g changes from 10^{-5} to 10^{-1}. The theoretical predictions for the dimensionless maximum permanent transverse displacements according to the bending only and shear and bending analyses are fairly similar in Figs 14 and 15. However, the transverse shear effect dominates the response of a beam when the impact point is close to a support since the maximum shear sliding deformation equals the total maximum permanent deformation when $v_1 \leqslant 1$. The lines associated with the shear and bending analyses (②) in Figs 14 and 15 are terminated when the maximum shear sliding equals the beam thickness[9].

The influence of the membrane force in a theoretical solution becomes increasingly important with larger external dynamic energies. Therefore, the bending only and shear and bending theoretical solutions are only valid for beams with axial restraints when the transverse deformations remain small.

The theoretical predictions in Section 3, obtained using the approximate square yield curve in Fig. 1(a), do bound those in Fig. 14 with a parabolic yield curve when the impact point is at the centre of the beam[7]. However, the theoretical analysis with the parabolic yield curve has not been developed when the impact point is at any position on a beam.

The theoretical analysis in Section 3 indicates that when the mass ratio g is small ($g/r^2 \ll 1$) the deformation of the beam during the phases with moving plastic hinges is very small. It transpires that almost all of the external dynamic energy is absorbed during the final phase of motion in which two parts of the beam rotate as rigid bodies about the supports. In this circumstance, the dimensionless maximum permanent transverse deformation can be expressed approximately as

$$\bar{W}_f = [-1+\sqrt{[1+2\iota\gamma/(1+r)]}]/2\gamma \tag{60}$$

which gives good agreement with the complete solution in Section 3, even when $g = 0.1$.

The various cases discussed in Section 2 are valid for different ranges of v_1 which are obtained from the associated static admissibility conditions. It can be shown that when $v_1 < 1$ the beam on the right-hand side of the impact point cannot rotate because $-M_0 < M < M_0$ for $z > 0^+$ and this behaviour is classified as Case III. When $v_1 > 1$, the theoretical analysis for Case III is no longer valid since $|M| > M_0$ at the clamped end. Therefore, a plastic hinge develops at the clamped end and the right-hand side of the beam rotates about the support. This behaviour is classified as Case II. It turns out that the theoretical analysis for Case II is not valid when $v_1 > 3$ since $|M| > M_0$ occurs at $z = z_1 < 1$. Thus, to overcome the difficulty when $v_1 > 3$, Case I is defined with a plastic bending hinge at $z = z_1$ and the beam in the region $z_1 < z < 1$ remains stationary because the shear force is zero at the location of the bending hinge at $z = z_1$.

The foregoing discussion shows that the transverse velocity profiles during the shear sliding phases depend only on the parameter v_1, or the length l_1 when Q_0 and M_0 are given. Similar deformation profiles can be obtained for the left-hand side of the beam with a different range of v_2, or a different length of l_2, which is assumed to be larger than l_1 in this paper without any loss in generality.

A complete theoretical solution which is valid for all values of the parameters including $v_2 < 3$ and $g > 3r^2/v_1$ will be presented in another paper.

5. CONCLUSIONS

The transverse shear and bending response and finite deflection behaviour of clamped beams struck transversely by a mass at any point of the span are examined in Sections 2 and 3, respectively. The transverse shear sliding and maximum permanent transverse deformations of a beam with, or without, axial restraints, can be obtained analytically. When the mass ratio g is small (i.e. large striking mass), the maximum permanent transverse deformation may be obtained from eqn (60).

Transverse shear forces may dominate the response when the impact point is close to a support, while membrane forces, or finite deflections, are important for maximum transverse deflections larger than the beam thickness, approximately.

Acknowledgements—The authors wish to thank the Science and Engineering Research Council for their partial support of this study through Grant GR/B/89737. Jianhui Liu wishes to express his gratitude to Huazhong University of Science and Technology for a leave of absence and to the University of Liverpool for a University Studentship. In addition, thanks are due to the British Council for some funds from the Academic Links with China Scheme between the Huazhong University of Science and Technology and the Department of Mechanical Engineering, University of Liverpool. The authors are also indebted to Mrs A. Green of the Department of Mechanical Engineering, University of Liverpool, for her preparation of the tracings.

REFERENCES

1. N. Jones, Reponses of structures to dynamic loading. In *Mech. Properties at High Rates of Strain* (Edited by J. Harding), Inst. of Physics Conf. Series No. 47, pp. 254–276. Institute of Physics, Bristol and London (1979).
2. N. Jones and J. G. de Oliveira, The influence of rotatory inertia and transverse shear on the dynamic plastic behaviour of beams. *J. Appl. Mech.* **46**, 303–310 (1979).
3. N. Jones and J. G. de Oliveira, Dynamic plastic response of circular plates with transverse shear and rotatory inertia. *J. Appl. Mech.* **47**, 27–34 (1980).
4. N. Jones and J. G. de Oliveira, Impulsive loading of a cylindrical shell with transverse shear and rotatory inertia. *Int. J. Solids Structures* **19**, 263–279 (1983).
5. N. Jones and B. Song, Shear and bending response of a rigid-plastic beam to partly distributed blast-type loading. *J. Struct. Mech.* **14**, 275–320 (1986).
6. E. W. Parkes, The permanent deformation of an encastré beam struck transversely at any point in its span. *Proc. Instn Civ. Engrs* **10**, 277–304 (1958).
7. T. Nonaka, Some interaction effects in a problem of plastic beam dynamics, parts 1–3. *J. Appl. Mech.* **34**, 623–643 (1967).
8. P. S. Symonds, Plastic shear deformations in dynamic load problems. In *Engineering Plasticity* (Edited by J. Heyman and F. A. Leckie), pp. 647–664. Cambridge University Press, Cambridge (1968).
9. N. Jones, Plastic failure of ductile beams loaded dynamically. *Trans. ASME, J. Engng Ind.* **98**, 131–136 (1976).
10. N. Jones and J. H. Liu, Local impact loading of beams. *Proc. Int. Symp. on Intense Dynamic Loading and its Effects*, pp. 444–449. Science Press, Beijing, China (1986).
11. N. Jones and C. Guedes Soares, Higher modal dynamic plastic behaviour of beams loaded impulsively. *Int. J. Mech. Sci.* **20**, 135–147 (1978).
12. N. Jones, Dynamic behaviour of ideal fibre-reinforced rigid-plastic beams. *J. Appl. Mech.* **43**, 319–324 (1976).
13. A. J. M. Spencer, Impulsive loading of fibre-reinforced rigid-plastic plates. *Int. J. Engng Sci.* **17**, 35–47 (1979).
14. P. S. Symonds and N. Jones, Impulsive loading of fully clamped beams with finite plastic deflections and strain-rate sensitivity. *Int. J. Mech. Sci.* **14**, 49–69 (1972).
15. P. S. Symonds and T. J. Mentel, Impulsive loading of plastic beams with axial constraints. *J. Mech. Phys. Solids* **6**, 186–202 (1958).
16. N. Jones, A theoretical study of the dynamic plastic behaviour of beams and plates with finite-deflections. *Int. J. Solids Structures* **7**, 1007–1029 (1971).
17. J. G. de Oliveira, Beams under lateral projectile impact. *Proc. ASCE J. Engng Mech. Div.* **108**, 51–71 (1982).
18. S. R. Reid and S. R. Hendry, Impact response of fluid-backed metal beams. *Comput. Struct.* **20**, 321–338 (1985).
19. N. Jones, Bounds on the dynamic plastic behaviour of structures including transverse shear effects. *Int. J. Impact Engng* **3**, 273–291 (1985).
20. J. H. Liu and N. Jones, Experimental investigation of clamped beams struck transversely by a mass. *Int. J. Impact Engng* **6**, 303–335 (1987).